JGR Atmospheres

RESEARCH ARTICLE
10.1029/2020JD033306

On the Interdecadal Variation of the Warm Water Volume in the Tropical Pacific Around 1999/2000

Xiaofan Li[1,2], Zeng-Zhen Hu[3], Bohua Huang[4], and Fei-Fei Jin[5]

[1]Key Laboratory of Geoscience Big Data and Deep Resource of Zhejiang Province, School of Earth Sciences, Zhejiang University, Hangzhou, Zhejiang, China, [2]Southern Marine Science and Engineering Guangdong Laboratory (Zhuhai), Zhuhai, Guangdong, China, [3]Climate Prediction Center, NCEP/NWS/NOAA, College Park, MD, USA, [4]Department of Atmospheric, Oceanic, and Earth Sciences, College of Science, George Mason University, Fairfax, VA, USA, [5]Department of Atmospheric Sciences, University of Hawaii at Manoa, Honolulu, HI, USA

Abstract A profound change in the variations of warm water volume (WWV) of the tropical Pacific occurred around 1999/2000, coincided with the interdecadal shift of the El Niño–Southern Oscillation (ENSO) properties to a higher frequency and smaller amplitude regime. The persistence of WWV is decreased for all calendar months since 2000, associated with a decrease in its variance and an increase in its frequency. Moreover, the WWV-sea surface temperature relationship associated with the ENSO cycle is weakened during 2000–2019, implying that the recharge/discharge process is less efficient in driving the phase transition of an ENSO cycle and ENSO became less periodical compared with that during 1979–1999. Corresponding to the weaker precursory connection of WWV to ENSO, the geographical origin of precedent thermocline anomalies has shown a northwestward migration since 2000. This is consistent with the suppression of the equatorial air-sea feedback and the systematical northwestward shift of the atmosphere-ocean coupling center in the tropical Pacific. Changed annual cycle and enhanced zonal contrast of sea surface temperature in the equatorial Pacific may be connected with the interdecadal variations of the ENSO and WWV features.

Key Points:
- Amplitude and persistence decreases and northwestward shift of WWV since 2000
- Less efficient of the recharge/discharge process in driving the phase transition of an ENSO cycle since 2000
- Less periodical and more irregular ENSO cycle since 2000

Correspondence to:
X. Li,
xiaofanli@zju.edu

Citation:
Li, X., Hu, Z.-Z., Huang, B., Jin, F.-F. (2020). On the interdecadal variation of the warm water volume in the tropical Pacific around 1999/2000. *Journal of Geophysical Research: Atmospheres*, *125*, e2020JD033306. https://doi.org/10.1029/2020JD033306

Received 15 JUN 2020
Accepted 23 AUG 2020
Accepted article online 31 AUG 2020

Author Contributions:
Formal analysis: Xiaofan Li, Zeng-Zhen Hu
Funding acquisition: Xiaofan Li
Methodology: Zeng-Zhen Hu
Supervision: Zeng-Zhen Hu
Writing - original draft: Xiaofan Li, Zeng-Zhen Hu
Writing – review & editing: Zeng-Zhen Hu, Bohua Huang, Fei-Fei Jin

1. Introduction

Predictability of global climate variability at interseasonal-to-interannual time scales largely relies on the tropical forcing associated with the El Niño–Southern Oscillation (ENSO), a coupled irregular oscillation in the tropical Pacific (Hu, Kumar, Jha, & Huang, 2020; National Research Council, 2010; Wang et al., 2016). Spatially, ENSO is characterized by a variety of sea surface temperature (SST) patterns in the tropical Pacific, such as coastal, eastern (EP), and central Pacific (CP) El Niño, as well as uncoupled El Niño with small contrast of the SST warming between the central and eastern tropical Pacific (e.g., Hu et al., 2019; Hu, McPhaden, Kao & Yu, 2009; Kug et al., 2009; Kumar, et al., 2020). Temporally, though fundamentally an interannual phenomenon with time scales ranging from 2 to 7 years, the dominant frequency and the amplitude of ENSO vary from decades to decades. For example, the ENSO variability switched from a near-biennial high-frequency regime with moderate strength during 1962–1975 to an almost quadrennial low-frequency regime with enhanced strength during 1980–1999 (An & Wang, 2000; Wang, 1995). It was then returned to a high-frequency regime with reduced variability since 2000 (Horii et al., 2012; Hu et al., 2016; Hu, Kumar, Huang, et al., 2020; Hu, Kumar, Zhu, et al., 2017; Kumar & Hu, 2014; McPhaden, 2012).

The interdecadal shift between the latter two periods (1979–1999 vs. 2000–2019) is visible in vital ENSO indicators, including the warm water volume (WWV) index in the tropical Pacific (e.g., Meinen & McPhaden, 2000) and the Niño3.4 index (Figure 1a). Although the WWV is derived from the reanalyzed ocean temperature anomalies from the Global Ocean Data Assimilation System (GODAS; Behringer, 2007; to be described in section 2), its interdecadal shift is robust since the results are similar to the calculations based on the ocean temperature profiles from the Tropical Atmosphere Ocean (TAO) moorings (not shown; the TAO-based WWV index data are available at http://www.pmel.noaa.gov/tao/wwv/data/wwv.dat; Meinen & McPhaden, 2000). Associated with the amplitude and frequency changes in ENSO (Figure 1c), the subsurface ocean temperature variability in the tropical Pacific also experienced significant changes around 1999/2000. As shown in Figure 1b (blue curve), the amplitude of the WWV fluctuation is decreased in almost all time scales in 2000–2019 (blue curve) in comparison with that in 1979–1999

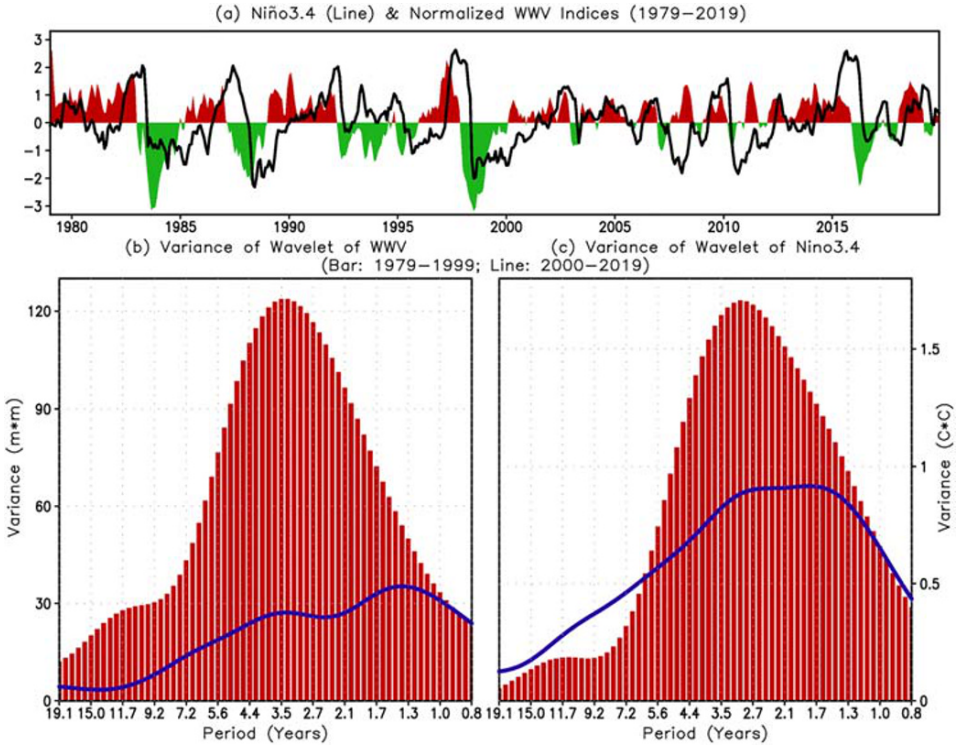

Figure 1. (a) Monthly mean Niño3.4 (line) and WWV (shading) indices from January 1979 to December 2019; variance dependence on time scales of the (b) WWV and (c) Niño3.4 indices for the average in January 1979 to December 1999 (bar) and January 2000 to December 2019 (curve), based on the time scale decomposition of wavelet (Hu & Nitta, 1996; Meyers et al., 1993). Panels (b) and (c) are replotted with updated data after Hu, Kumar, Zhu, et al. (2017) and Hu, Kumar, Huang, et al. (2020).

(red bars). Moreover, the periodicity is also weakened in the later period. The WWV index in 1979–1999 shows a predominant peak centered at around 3–4 years that contains most of the energy in the interannual frequency band; however, the variance in 2000–2019 is nearly flat in the frequency range of 1–5 years, with two weak peaks near 4 and 1.5 years, respectively. Similar changes are also seen for the Niño3.4 index (Figure 1c). This implies a shift of the ENSO regime around 2000 into a fluctuation almost without a dominant frequency. Visually, anomalous events occurred more frequently and had shorter durations since 2000 (Figure 1a), which we refer to as a high-frequency ENSO regime. As a result of the regime shift with the frequency increase and variance decrease, ENSO prediction skill decreased since 2000 (Barnston et al., 2012; Hu, Kumar, Huang, et al., 2020; Neske & McGregor, 2018; Wang et al., 2010). It has been noticed that this regime shift occurred on the background of enhancing contrasts of the atmospheric and oceanic mean states between the western and eastern tropical Pacific (England et al., 2014; Hu et al., 2016, 2017; Hu, Kumar, Huang, et al., 2020).

WWV is the major energy source for ENSO development and also one of the crucial precursors for ENSO forecast (Chen et al., 2020; Clarke & van Gorder, 2001; Hu, Kumar, Huang, et al., 2017; Izumo et al., 2019; Kug et al., 2005; McPhaden et al., 2006; Meinen & McPhaden, 2000; Tseng et al., 2016). Also, WWV is a proxy to describing the recharge/discharge process that link to the subsurface ocean heat exchange between the equator and off the equator that drive the phase transition of an ENSO cycle (Clarke & van Gorder, 2001; Hu, Kumar, Huang, et al., 2017; Izumo et al., 2019; Jin, 1997a, 1997b; Kug et al., 2005; Meinen & McPhaden, 2000; Singh & Delcroix, 2013; Tseng et al., 2016; Wyrtki, 1985). In the recharge/discharge paradigm, the phase transition of an ENSO cycle is controlled by the nonequilibrium between the surface zonal wind stress and the zonal mean equatorial thermocline depth (Jin, 1997a, 1997b). The heat budget analysis shows that both the thermocline feedback and the zonal advective feedback contribute to the ENSO phase transition (Ren & Jin, 2013). Although both CP and EP El Niños are associated with the recharge oscillator mechanism (Ren & Jin, 2013), the westward shift of the SSTA in the CP ENSO

and the presence of the easterly wind anomalies in the eastern equatorial Pacific reduce the positive feedback in the eastern Pacific. This scenario is consistent with the fact that the equatorial band WWV discharge during CP El Niño seems weaker than during EP El Niño (Singh & Delcroix, 2013). Therefore, understanding the interdecadal variation associated with WWV may help us to better understand the interdecadal shift of ENSO properties around 1999/2000 and the decline of ENSO prediction skill since 2000 (Barnston et al., 2012; Hu, Kumar, Huang, et al., 2020; Neske & McGregor, 2018; Wang et al., 2010).

In this work, as a complement of these previous studies about the regime shift of ENSO in 1999/2000, we emphasize the interdecadal variation of WWV in the tropical Pacific. The following topics are the focuses of our analysis: (a) What are the persistence changes of WWV around 1999/2000 and how are they associated with the WWV variance and frequency change? (b) What is the geographic change in the source of WWV associated with the ENSO regime shift? (c) What are the possible connections of the ENSO feature change with the change in annual cycle? The paper is organized as follows. The data used in the analysis are described in section 2; section 3 shows the changes of the persistence and variance of WWV; section 4 examines the differences of the evolution of the recharge/discharge process associated with the interdecadal variation of WWV; section 5 discusses a possible connection of the interdecadal variation of ENSO with annual cycle change; a summary with discussion is given in section 6.

2. Data

The data set analyzed in this work is mainly from GODAS (Behringer, 2007). GODAS is an ocean reanalysis of the National Environmental Prediction Center (NCEP) starting from 1979 and continuously updated in near real-time. Its first guess field is provided by the Geophysical Fluid Dynamics Laboratory modular ocean model, version 3 (MOM.v3), with a quasi-global configuration. The model domain extends from 75°S to 65°N and has a resolution of 1° by 1° with enhancement to 1/3° in the meridional direction within 10° of the equator. It has 40 vertical levels with a 10-m resolution in the upper 200 m. Both observed ocean temperature profiles, as well as synthetic salinity profiles constructed from the former based on local climatological temperature-salinity relation, are assimilated in a three-dimensional variational (3DVAR) data assimilation scheme. In the assimilation cycle, the MOM.v3 integration is forced by the surface momentum flux, heat flux, and freshwater flux from the NCEP atmospheric reanalysis 2 (NCEP2; Kanamitsu et al., 2002).

The depth of 20°C isotherm (D20) and surface wind stress from NCEP2 are analyzed. Following Meinen and McPhaden (2000), the WWV index is defined as the average of D20 from GODAS over the region of 5°S–5°N, 120°E–80°W. The Niño3.4 index is the SST anomalies averaged in the region of 5°S–5°N, 120–170°W (Barnston et al., 1997). The data duration is January 1979 to December 2019. In the calculations shown in Figures 1–7, the anomalies in each of the periods (January 1979 to December 2019, January 1979 to December 1999, and January 2000 to December 2019) are referred to the climatologies in the respective periods. The three periods are usually referred to as the early (1979–1999), later (2000–2019), and the whole (1979–2019) periods later on.

3. The Decline of the Persistence and Variance of the WWV Index

Figure 2 shows the persistence of the WWV index with respect to the initial calendar month and the lead month. For the whole period (black curves, Figure 2) and the early period (red curve, Figure 2), the WWV index lagged correlation generally decays from Year 0 to the midsummer of Year 1. This is especially true for the initial months in the earlier part of the year (e.g., January to May; Figures 2a–2e) when a relatively small peak occurs in late summer before further decay in subsequent months. Consistent with previous work (such as McPhaden, 2003), the WWV index does not show a spring persistence barrier (Figure 2), that is, a major dip of prediction skill followed by a recovery. The lack of spring barrier in WWV is different from that of the SST anomalies associated with ENSO, which has a pronounced spring persistence barrier (McPhaden, 2003; Torrence & Webster, 1998; Webster & Yang, 1992).

On the other hand, for the initial months after May, there is a stiffer decay of correlation starting from November, which can be seen in Figures 2h and 2i, corresponding to the initial months in August and September, respectively. There is also a recovery in the subsequent summer. Therefore, the WWV index displays a winter persistence barrier, as indicated in McPhaden (2003, see his Figure 2), although the WWV winter barrier is less pronounced than the spring barrier of the Niño SST indices (not shown).

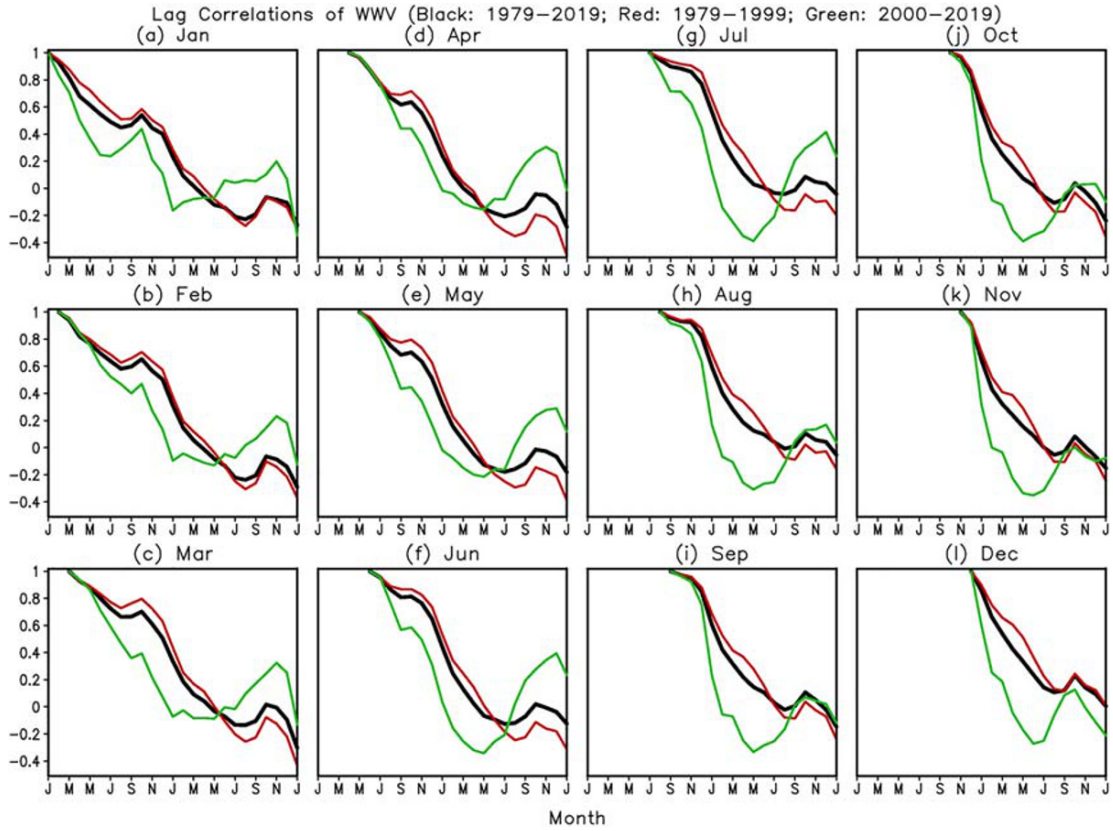

Figure 2. Lag correlations of the WWV index for each calendar month, based on data from January 1979 to December 2019 (black curve), from January 1979 to December 1999 (red curve), and from January 2000 to December 2019 (green curve).

McPhaden (2003) argued that the winter persistence barrier of ocean heat content is linked to a seasonal reduction of the variance of heat content. Here we confirm that the WWV index has the smallest variance in boreal winter months and comparable variance in the other three seasons in 1979–2019 (see the black line in Figure 3).

In comparison to the WWV persistence in 1979–1999, the persistence of the WWV index decreases at a faster rate in the summer and fall of Year 0 during 2000–2019 (green curves, Figure 2), which generally does not show secondary peak as seen in the earlier period. As a result, the correlation is usually at a minimum in the spring and early summer of Year 1 and then rebounds in the fall and winter of Year 1. This rebound appears more noticeable for all calendar months during 2000–2019 (green line) compared with that during 1979–1999 (red line, Figure 2). For certain initial months (e.g., Figures 2e–2g), the rebound correlations may reflect the more frequent occurrence of the re-emergent La Niña events in the later period (e.g., Hu et al., 2014).

The reduction in the persistence of the WWV index is linked to the frequency increase of ENSO after 1999/2000 (Hu, Kumar, Huang, et al., 2020; Hu, Kumar, Zhu, et al., 2017). After the regime shift in 1999/2000, the maximum variability of the Niño3.4 index is shifted from being contained in the period band of 1.5–5 years during 1979–1999 to smaller peaks being more confined around 1.5–3.5 years since 2000 (Figure 1c). Due to the weakening of the lower-frequency components, the whole frequency band shows a flatter variance distribution. Similarly, the WWV index also displayed almost no peak since 2000 so that its variability is closer to a white noise process (Figure 1b). The decline of the persistence of WWV may degrade the role of the subsurface ocean temperature anomalies as a precursor to make ENSO prediction (Horii et al., 2012; McPhaden, 2012; Wen et al., 2014). This may be a key factor leading to the decline of ENSO prediction skill after 20,000 (Barnston et al., 2012; Hu, Kumar, Huang, et al., 2020; Izumo et al., 2019; Neske & McGregor, 2018).

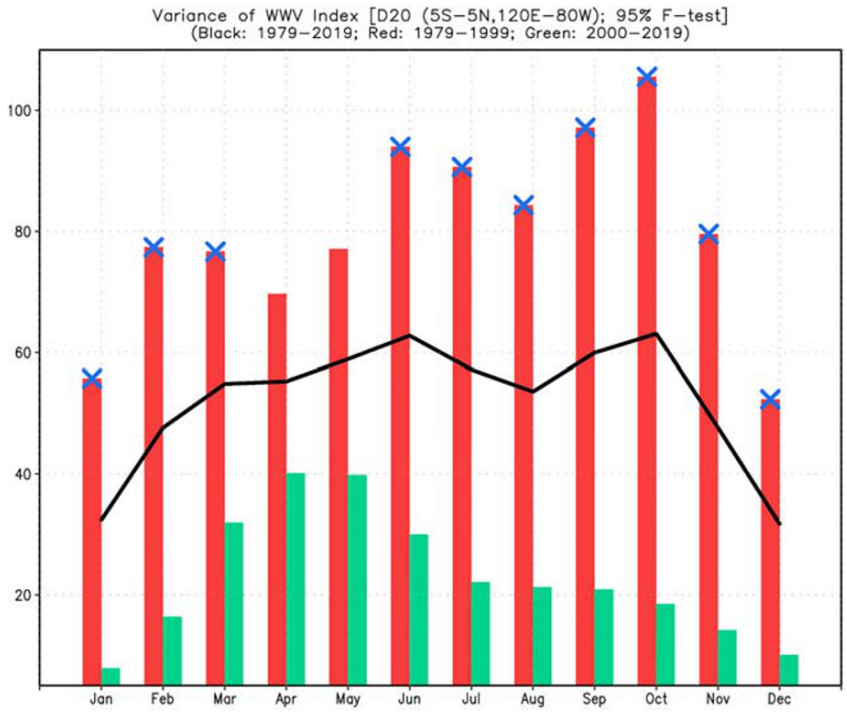

Figure 3. Annual cycle of the variance of WWV index during January 1979 to December 2019 (black line), January 1979 to December 1999 (red bars), and January 2000 to December 2019 (green bars). The unit is m^2. The bars with blue multiplication represent the differences of the variances between January 1979 to December 1999 and January 2000 to December 2019 significant at the 95% level using an *F* test.

The decrease of the persistence of the WWV index during 2000–2019 is associated with a significant decrease of its variability amplitude during 2000–2019 (green bars, Figure 3) compared with that during 1979–1999 (red bars, Figure 3). This is consistent with the previous argument that strong (weak) persistence is linked to the large (small) amplitude of variability of WWV (McPhaden, 2003). The persistence and magnitude changes of the WWV variability reflect the fact that ENSO has shorter time scale and weaker strength during this period.

Meanwhile, the seasonality of the WWV variations was also changed. Its maximum variance switched from June–October during 1979–1999 (red bars, Figure 3) to March–June during 2000–2019 (green bars, Figure 3) although the minimum variance of WWV remains in December and January. The decadal shift of WWV seasonality may be associated with the overall weakening of low-frequency precursory signal for 2000–2019. The weak WWV variability elevates the relative importance of the higher frequency variability in the atmosphere that peaks in boreal spring and then affects the subsequent WWV evolution. For instance, McPhaden et al. (2006) developed a regression model to predict boreal winter Niño3.4 SST using previous WWV index and the intraseasonal wind variance in the western Pacific (primarily related to the Madden-Julian Oscillation, MJO). They found that the maximum influence of the MJO on the winter Niño3.4 was in the previous boreal spring (April–June). They also noted that WWV and MJO forcing variations were positively correlated. These factors suggest the scenario that large-scale oceanic intraseasonal Kelvin waves in response to the MJO forcing can impact the subsequent WWV estimates. Later, Neske and McGregor (2018) showed explicitly how the higher frequency noise forcing related to episodic winds enters into the WWV estimates.

4. Weakened Connection With WWV and the Geographical Origin Shift

The differences in the persistence of the WWV index during 1979–1999 and 2000–2019 are associated with the different evolutions of the recharge/discharge process. Figure 4 shows the lagged correlations of the WWV index with the precedent D20 anomalies up to 1-year lead at a 2-month interval during 1979–1999 (left panels) and 2000–2019 (right panels). When D20 leads the WWV index by 12 months, the significant positive correlations are present in the western and central tropical Pacific and significant negative correlations in

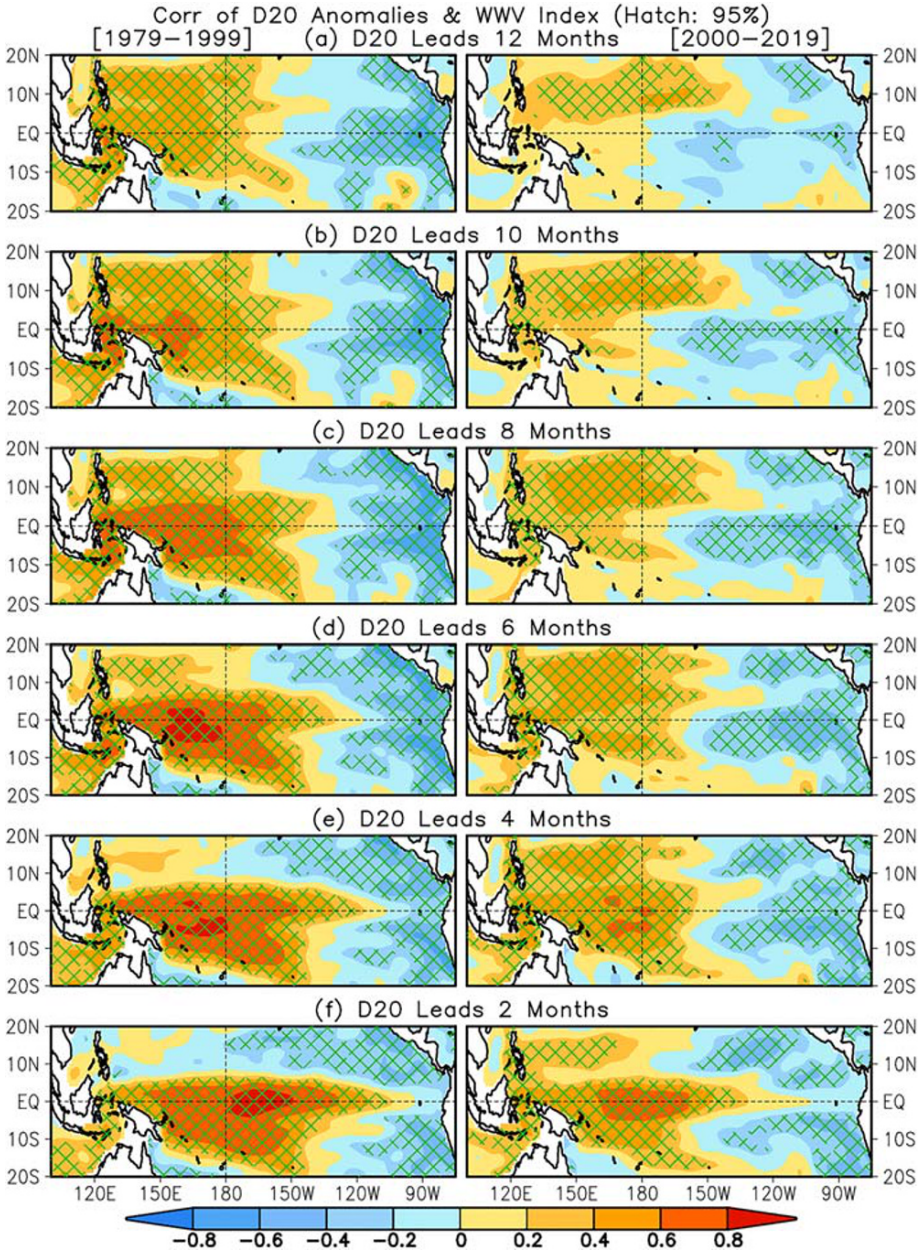

Figure 4. Correlations between D20 anomalies and the WWV index during January 1979 to December 1999 (left panels) and January 2000 to December 2019 (right panels) for D20 anomalies leading the WWV index by 12, 10, 8, 6, 4, and 2 months. The hatched regions are significant at the level of 95% using a Student's *t* test with estimated independent sample sizes.

the eastern tropical Pacific as well as along the American coast during 1979–1999 (hatches, left panel of Figure 4a). During 2000–2019 (right panel of Figure 4a), the significant positive correlations are seen only on the northern side of the equator along 10°N in the western Pacific and the negative correlations are insignificant in the eastern Pacific. In both periods, a dipole-like pattern of the subsurface ocean temperature anomalies between the warm west and cold east appears in the equatorial Pacific, suggesting that the ocean is dominated by the tilt mode in a La Niña state (Clarke, 2010; Kumar & Hu, 2014). However, compared with that in 2000–2019 (right panels of Figures 4a–4d), the overall spatial distribution of the correlation pattern is more meridionally symmetric with respect to the equator in 1979–19,999 (left panels of Figure 4(a)-(d)).

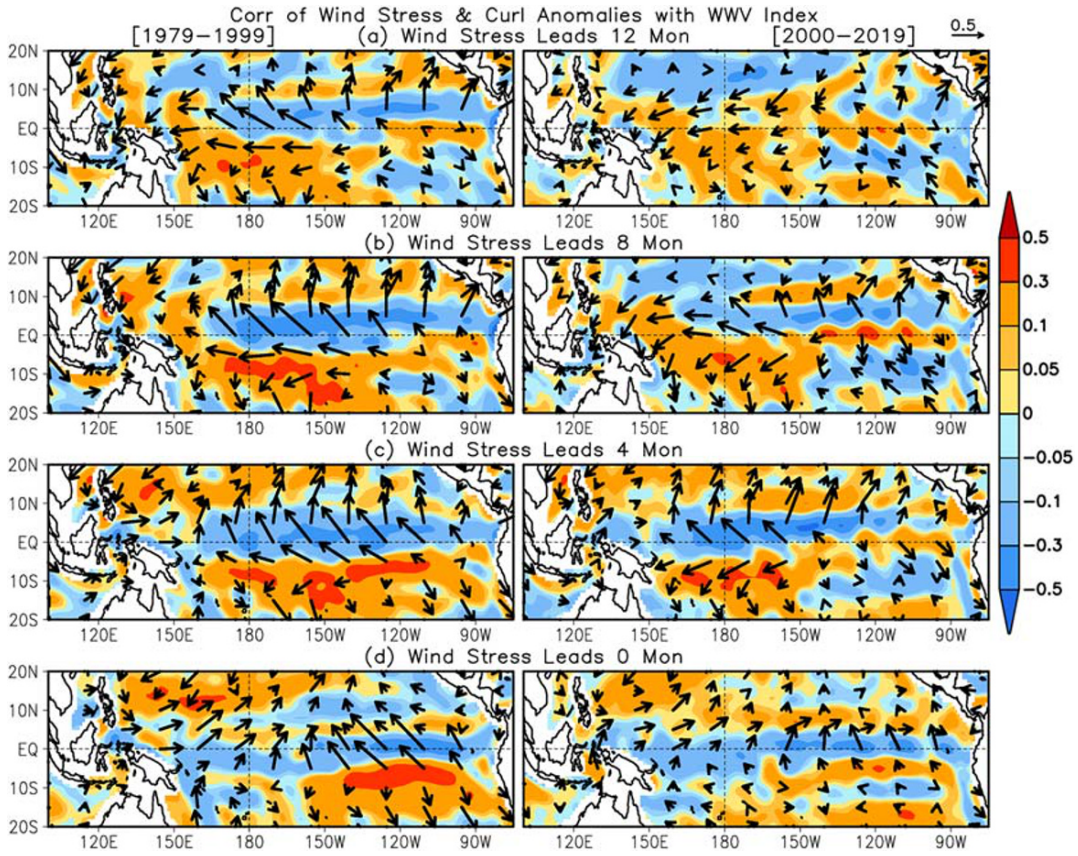

Figure 5. Correlations of surface wind stress (vectors) and its curl (shading) anomalies with the WWV index during January 1979 to December 1999 (left) and January 2000 to December 2019 (right) for D20 anomalies leading the WWV index by (a) 12, (b) 8, (c) 4, and (d) 0 months.

When the lead-time shortens from 12 to 2 months, the area of significant positive correlation in the western equatorial Pacific expands eastward while that of the significant negative correlation along the equator gradually vanishes during 1979–1999 (left panels of Figures 4b–4f). This features the growth of the WWV mode that gradually replaces the tilt mode. During 2000–2019, a substantial area of the significant negative correlations appears in the 8-month lead (right panels of Figure 4c) while the significant positive correlations still maintained north of the equator (hatches, right panels of Figures 4b and 4c). In the next 4 months, the positive correlation area migrates gradually from the northwestern Pacific to the equator (right panels of Figures 4d–4f) and becomes centered near the equator at a 2-month lead (hatches, right panels of Figure 4e). Such distinct evolution suggests a distinctive geographical origin of the precedent ocean heat storage in 8–12 month leads (Figures 4a–4c) associated with WWV variability: it is changed from the western tropical Pacific during 1979–1999 to the northwestern tropical Pacific during 2000–2019.

Some of these D20 differences between the early and later periods may be attributable to the different characteristics of the surface wind stresses as shown in the WWV index correlations with the surface wind stress (vector) and stress curl (shading) anomalies in Figure 5. Although the patterns of wind stress and stress curl are somewhat similar between the early (left panels) and later (right panels) periods at the 4-month lead (Figure 5c) and contemporary (Figure 5d) correlations, they are more distinctive at 12- and 8-month leads. At 12-month lead (Figure 5a), in the circumstance of positive WWV, the correlations suggest that the easterly wind stress anomalies prevail between the equator and 10°N to the west of 150°W during 2000–2019 (right panel, Figure 5a) while it is the southeasterly wind anomalies during 1979–1999 (left panel, Figure 5a). This difference in wind patterns persists until 4 months later (Figure 5b). In 2000–2019, the persistent easterly wind stress anomalies over the north of the equator promote Ekman convergence in the northwestern Pacific near 10°N. In 1979–1999, however, the southerly component of the winds to the north of the

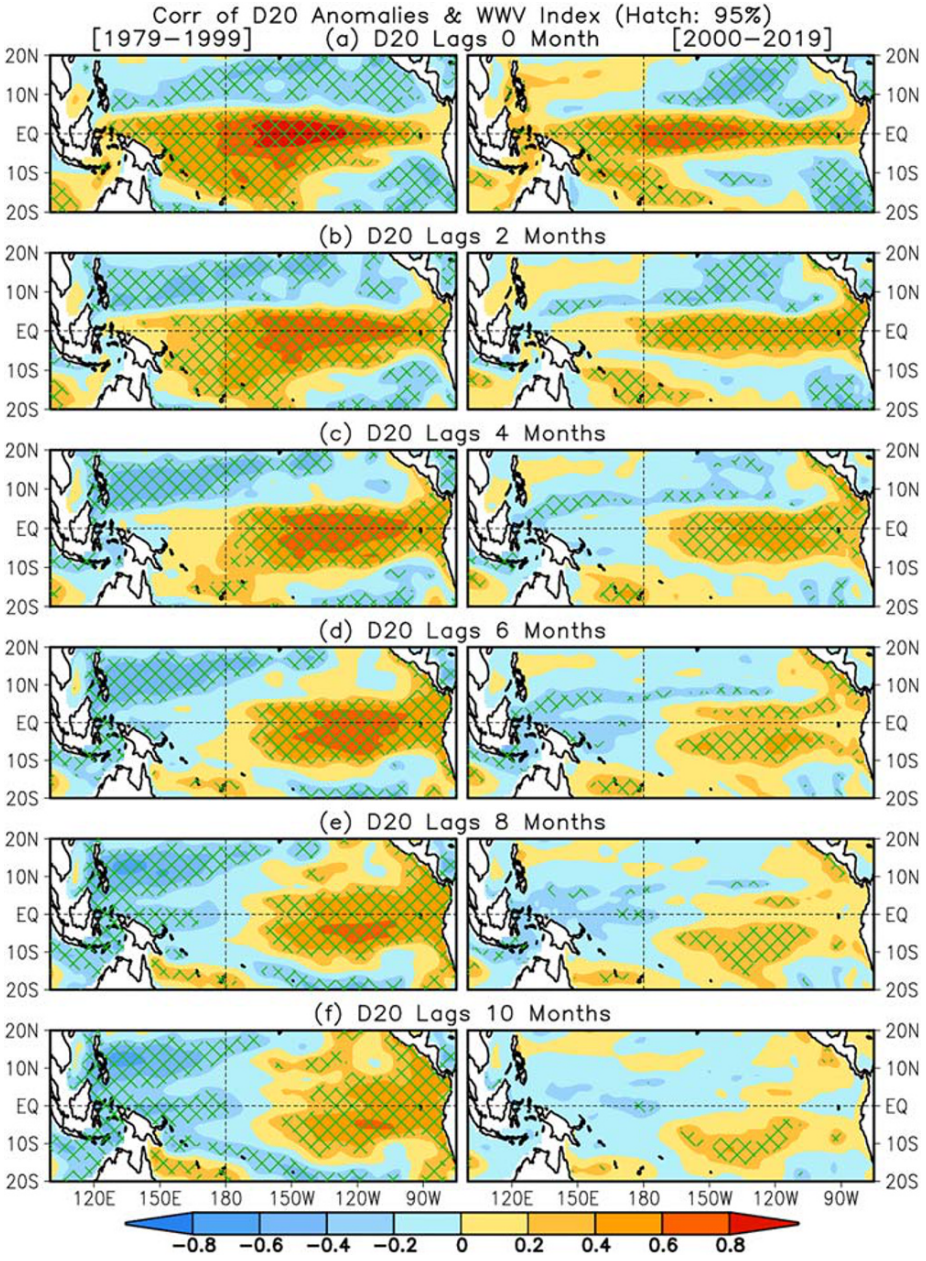

Figure 6. Correlations between D20 anomalies and the WWV index during January 1979 to December 1999 (left panels) and January 2000 to December 2019 (right panels) for D20 anomalies lagging the WWV index by 0, 2, 4, 6, 8, and 10 months. The hatched regions are significant at the level of 95% using a Student's *t* test with estimated independent sample sizes.

equator promotes a more eastward Ekman transport and prevents convergence in the northwestern Pacific. As a result, the northward displacement of the heat storage site during 2000–2019 may reduce its efficiency in supplying the heat content for the ENSO cycle. Battisti (1989) argued that the essential oceanic wave signals for ENSO are confined in 8°S–8°N. Off-equatorial Rossby waves outside this latitude band play a relatively weak role in triggering ENSO.

At lead month 0, the significant positive correlations span almost the entire equatorial Pacific (Figure 6a), suggesting that the peaking WWV is associated with the deepened thermocline in the central equatorial Pacific. To some extent, the spatial distribution pattern in Figure 6a is analogous with that of D20 anomalies during the development phase of an El Niño (see Figure 6 of Singh & Delcroix, 2013). The

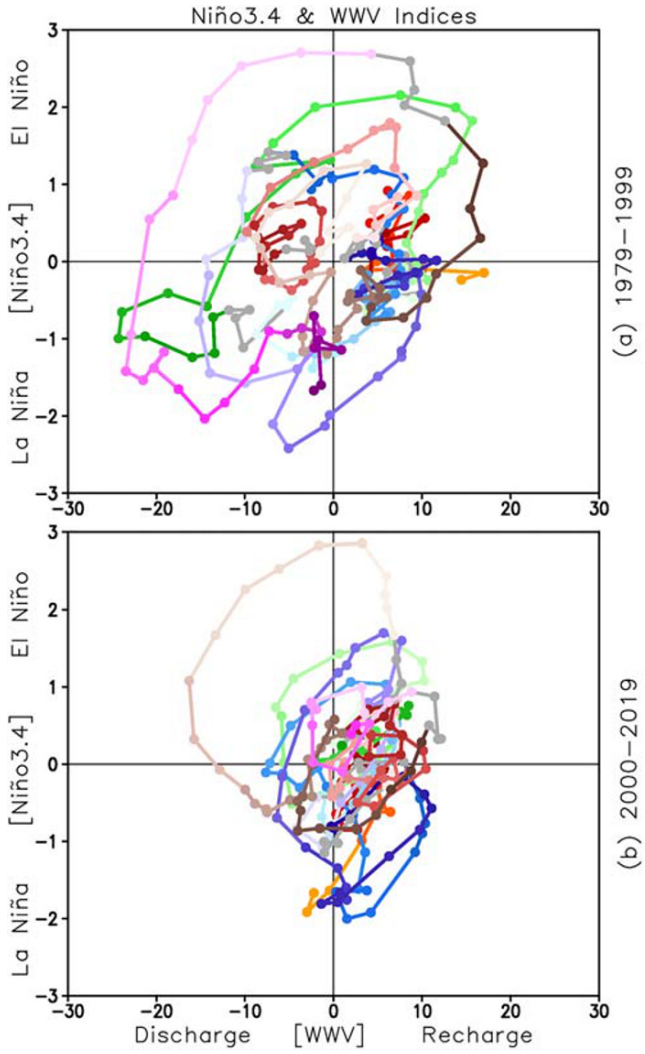

Figure 7. Phase orbits of the monthly mean WWV (*x* axis; m) and Niño3.4 (*y* axis; °C) indices during (a) January 1979 to December 1999 and (b) January 2000 to December 2019.

results are similar to those derived from 10-year high-pass filtered data (not shown), suggesting that the processes shown here reflect the interseasonal-interannual variations.

Four months after the WWV peak, the area of significant positive correlation in the central-eastern Pacific (90°W–150°W) is shrinking zonally on the equator, in company with the two flanking off-equatorial bands (Figure 6c). According to Chen et al. (2016), this is a sign that the off-equatorial D20 anomalies associated with the reflected Rossby waves from the eastern boundary dominate over the equatorial D20 anomalies. In this situation, a reversal of the equatorial zonal current further weakens the eastern equatorial SST anomalies. Indeed, the area of significant positive correlation has moved off the equator with no significant correlation along the equator and shrank substantially 6 months afterward (right panels, Figures 6d–6f). An area of high positive correlation (>0.6) is largely symmetric to the equator in the eastern Pacific in 4 (Figure 6c) to 6 (Figure 6d) months after the WWV peak, suggesting strong Bjerknes feedback during this period.

During 2000–2019 (right panels of Figure 6), the amplitudes of the positive correlation of the WWV index with D20 anomalies in the tropical Pacific are smaller than that during 1979–1999 (left panels of Figure 6). In addition to the overall decline of the correlations during 2000–2019, the evolution of the spatial distribution of D20 anomalies lagging the WWV index also shows distinct features between the two periods (Figures 6b–6f). For instance, when D20 lags the WWV index by more than 6 months (Figures 6d–6f), the positive correlations along the equator remain significant during 1979–1999 (left panels) but become insignificant during 2000–2019 (right panels). In the later period, statistically significant signals seem to be off-equatorial mostly and propagate westward as Rossby waves. The quick disappearance of the significant positive correlations is consistent with the increase of the ENSO frequency (Hu, Kumar, Huang, et al., 2020; Hu, Kumar, Zhu, et al., 2017) and the decrease of the persistence of the WWV index since 2000. Meanwhile, the correlations in the northwestern Pacific are negative and significant when D20 lags the WWV index by 2–10 months.

Spatially, the precedent and contemporary D20 anomalies show a westward migration of the significant positive correlations to the WWV index in the tropical Pacific during 2000–2019 compared with that during 1979–1999. Such northwestward shift is evident in the correlation patterns for the D20 anomalies leading the WWV index by 2–12 months (Figure 4). This scenario is consistent with the suppression and systematical northwestward shift of the atmosphere-ocean coupling region in the tropical Pacific indicated by Hu et al. (2013), Hu, Kumar, Huang, et al. (2020), Xiang et al. (2013), Lübbecke and McPhaden (2014), Bunge and Clarke (2014), and Li et al. (2019). According to An and Wang (2000), the zonal migration of the atmosphere and ocean coupling region affects the frequency of ENSO: westward shift (eastward extension) favors higher (lower) frequency of ENSO. Thus, the westward shift of the atmosphere-ocean coupling region since 2000 is a crucial factor causing the frequency increase of ENSO and lead-time shortening of WWV to ENSO (Hu, Kumar, Huang, et al., 2020; Hu, Kumar, Zhu, et al., 2017; McPhaden, 2012).

Overall, the lead and lag correlations of the WWV index with D20 anomalies are weaker during 2000–2019 than during 1979–1999. This reflects a suppression of the atmosphere-ocean coupling in the tropical Pacific since 2000. Figure 7 presents the phase diagram between the Niño3.4 and WWV indices, which clearly shows that the amplitude of ENSO events is smaller during 2000–2019 (Figure 7b) than during 1979–1999 (Figure 7a). According to Jin (1997), the ellipticity of a recharge oscillator trajectory in the phase diagram

depends on the lag between SSTA and thermocline depth anomaly (WWV). Since the trajectories in both Figures 7a and 7b generally form elliptic shapes with similar tilts although the latter is smaller, this seems to suggest that the recharge/discharge process plays some roles in both periods. On the other hand, in comparison to the early period, individual trajectories in the later period are more disorganized and less centered at the origin. This disorganization is consistent with the reduced maximum WWV-Niño3.4 correlation in the later period.

The reduction of the WWV variability since 2000 (Figures 3 and 7), together with the significant decline of the positive correlation when the WWV index leads the Niño3.4 index (see Figure 2b of McPhaden, 2012; Figure 2 of Hu, Kumar, Zhu, et al., 2017; Figure 10 of Hu, Kumar, Huang, et al., 2020), implies a less efficient recharge/discharge process in driving the ENSO phase transition during 2000–2019 than during 1979–1999. This suggests that the oscillation was more irregular and ENSO evolution was less periodical (Figure 1c) (Kessler, 2002).

5. A Possible Connection With the Changed Annual Cycle

Here we explore whether the annual cycle on the equator is modified in such a way that it undermines the coupling strength in the central-eastern equatorial Pacific. The contours in Figure 8 show the Hovmöller diagrams for the monthly climatology of D20 (Figure 8a) and SST (Figure 8b) over the equatorial Pacific during 1979–1999. The strong zonal slope of D20 is linked to the zonal gradient of SST with warm SST in the western and cold SST in the eastern tropical Pacific and easterly wind stress (not shown) (110°W-Dateline). There is a distinctive SST annual cycle in the eastern equatorial Pacific, with the onset of the cold tongue in May–July followed by seasonal warming in March and April (contours, Figure 8b), while the thermocline has been shoaling gradually from January to August in the eastern Pacific (contours, Figure 8a).

Compared with the mean state in 1979–1999, the equatorial thermocline is generally deeper by 8 to 12 m to the west of 160°W throughout the year during 2000–2019 (shading, Figure 8a). Correspondingly, the SST is also warmer by 0.3–0.8°C to the west of the Dateline (shading, Figure 8b). Further to the east, however, differences of D20 and SST between the two periods become more seasonally dependent. The shoaling of the thermocline and the cooling of the SST in the eastern equatorial Pacific only occur in boreal early spring and winter while the D20 and SST differences between the two periods are mainly positive 120°W westward during boreal summer and fall. This means that the enhanced zonal contrast mostly occurs in boreal early spring and winter but not in summer and fall. In fact, the annual cycle is weakened in 2000–2019 in comparison to that in 1979–1999, as shown by the annual cycle departure from the annual mean in each of the respective periods (Figures 8c and 8d). The differences of D20 and SST between 2000–2019 and 1979–1999 are largely out of phase with the annual cycle in 1979–1999. Also, the largest annual cycle change occurs in the central-eastern equatorial Pacific (120–160°W).

Since ENSO is strongly phase-locked with the annual cycle with initiative in boreal spring or/and summer and peaking in boreal winter, most of its unstable growth due to Bjerknes feedback occurs during summer and fall over a background of strong zonal contrast along the equatorial Pacific provided by the climatological annual cycle there. The reduced annual cycle in 2000–2019, especially in boreal summer and autumn, may weaken the background state within the seasonal window of ENSO growth. Therefore, the ENSO events become weaker and last for a shorter period since 2000 even though the annual mean zonal contrast seems enhanced in the equatorial Pacific. This implies that the long-term trend of the seasonal cycle in the eastern equatorial Pacific may play an important role in modulating the ENSO amplitude variation.

6. Summary and Discussion

In this work, we investigated the interdecadal variation of WWV around 1999/2000 with a focus on its persistence and geographical origin. Coincided with the interdecadal shift of ENSO properties, the persistence of the WWV index is decreased for all calendar months during 2000–2019 compared with that during 1979–1999. The decrease of the persistence of the WWV index during 2000–2019 is associated with the decrease in the magnitude of the WWV variability and the increase in its frequency during 2000–2019. This is linked to the interdecadal shift of ENSO properties featured by a decrease of variability and an increase of frequency since 2000. Overall, both the recharge/discharge process associated with the ENSO cycle were suppressed, suggesting that the recharge/discharge process are less efficient in driving phase transition of an ENSO

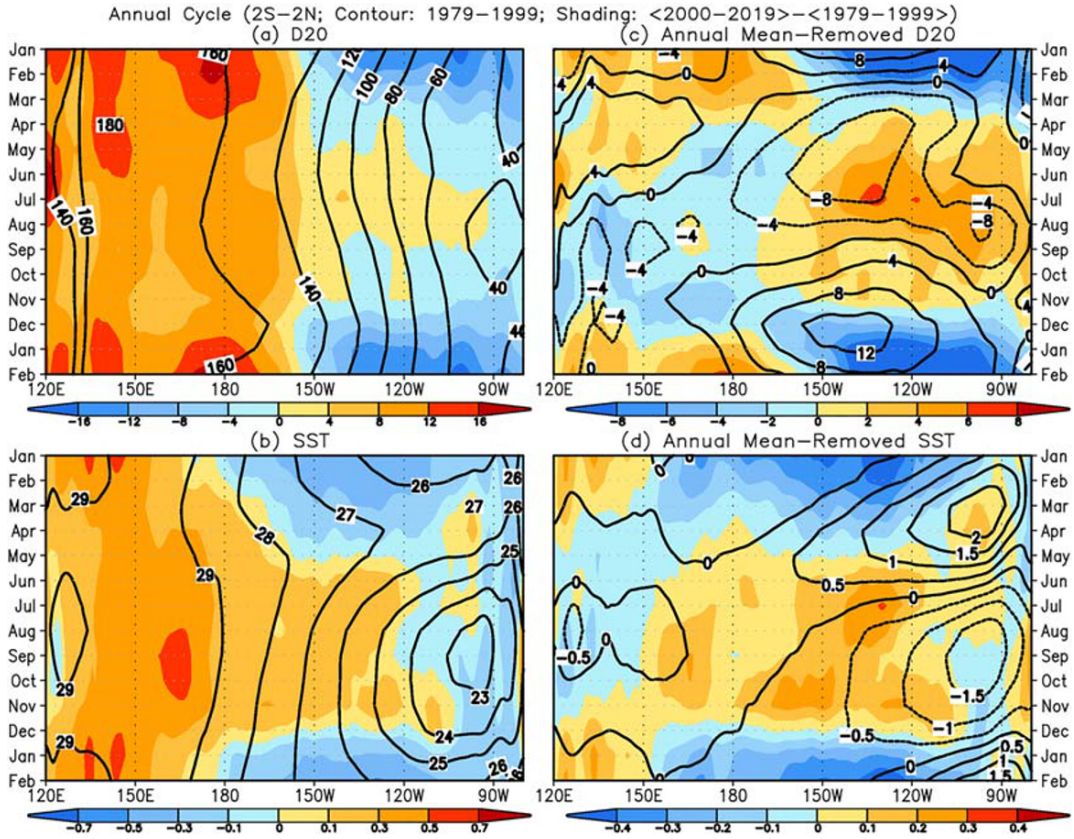

Figure 8. Annual cycle of (a) D20 and (b) SST and annual mean-removed annual cycle of (c) D20 and (d) SST averaged in 2°S–2°N for the mean in January 1979 to December 1999 (contours) and the difference of the mean in January 2000 to December 2019 minus the mean in January 1979 to December 1999 (shading). (c, d) The results with annual mean removal. The units are m for D20 and °C for SST.

cycle. As a result, the cyclic oscillation of ENSO was even more irregular, and ENSO evolution was less periodical during 2000–2019 compared with that during 1979–1999.

In addition to the weakening of the connection, the geographic origin of precedent thermocline (D20) anomalies associated with the WWV index shows a northwestward migration during 2000–2019. This is consistent with the suppression and a systematical northwestward shift of the atmosphere-ocean coupling region in the tropical Pacific. The westward shift of the atmosphere and ocean coupling leads to a shortening of the period of ENSO (An & Wang, 2000; Hu, Kumar, Zhu, et al., 2017; Li et al., 2019) and, consequently, to a decrease of the persistence of the subsurface ocean temperature anomalies in the tropical Pacific. Zhang et al. (2019) argued that the decadal change of the ENSO periodicity was associated with the predominance of either eastern Pacific or Central Pacific ENSO in the different decades, leading to the changes in the phase relationship between WWV and ENSO SST.

As a result of the interdecadal variations of WWV and ENSO, ENSO prediction skill decreased since 2000 (Barnston et al., 2012; Hu, Kumar, Huang, et al., 2020; Izumo et al., 2019; Neske & McGregor, 2018; Wang et al., 2010). For example, Barnston et al. (2012) documented that on average, the skills of 20 prediction models (12 dynamical and 8 statistical) were lower for the real-time forecasts during 2002–2011 than for the hindcasts in the 1980s and 1990s. They further argued that decadal variations in the ENSO feature are a greater skill-determining factor than the steady but gradual trend toward improved ENSO prediction science and models. Neske and McGregor (2018) further attributed the ENSO forecast skill decline post-2000 to the partition change of instantaneous wind response of ocean versus slow adjusted oceanic process.

The change in ENSO regime occurred on the background of an enhanced zonal contrast of the atmospheric and oceanic mean states in the tropical Pacific (England et al., 2014; Hu et al., 2016; Hu, Kumar, Huang, et

al., 2020; Hu, Kumar, Zhu, et al., 2017). However, the connection of the mean state change with ENSO regime shift is not straightforward (Chen & Jin, 2020). It can be argued that a strengthened zonal slope of the mean equatorial thermocline corresponds to an increase in ocean available potential energy and thus stronger ENSO activity (e.g., Goddard & Philander, 2001). On the other hand, as discussed in the previous section, an enhanced zonal contrast of SST across the tropical Pacific may push the active coupling area westward, leading to a change of ENSO features: decreasing its amplitude and increasing its frequency. With numerical experiments, Hu et al. (2013) argued that a combination of a steeper thermocline slope with stronger surface trade winds is linked to a smaller amplitude of ENSO. The enlarged zonal contrast of the background SST in the tropical Pacific may also enhance the zonal advective feedback, which brings SST anomaly center shifted to the west and increases the frequency of ENSO. Meanwhile, the reduced annual cycle in the eastern equatorial Pacific in 2000–2019 may narrow down the seasonal window of the background state favoring ENSO growth, leading to weaker growth of atmospheric and oceanic coupled anomaly in the tropical Pacific and a reduction of ENSO amplitude.

A follow-up question is what leads to the weakening of the eastern equatorial Pacific annual cycle from 1979–1999 to 2000–2019? Since the tropical Pacific annual cycle is determined by active ocean-atmosphere feedback (e.g., Köberle & Philander, 1994; Mitchell & Wallace, 1992; Xie, 1994), this might, in turn, be caused by the change of annual mean state due to multidecadal variability. McPhaden et al. (2011) noted that difference of the mean conditions in the tropical Pacific between 2000–2010 and 1980–1999 were opposite to that expected from greenhouse gas forcing in climate models. They argued that the asymmetric spatial structures of CP and EP El Niños during 1980–2010 may contribute to the changes in the background states. Since the change in the annual cycle is a potential factor associated with the decadal modulation of ENSO, it should be further explored in the framework of multidecadal variability in future studies.

Data Availability Statement

For data used in this study, you can download from https://www.esrl.noaa.gov/psd/data/gridded/data.godas.html or contact us via xiaofanli@zju.edu.cn website.

Acknowledgments
The authors thank the constructive suggestions from the reviewers. This paper complies with the AGU Publications Data Policy. X. L. was supported by the National Natural Science Foundation of China (41930967 and 41775040). B. H. is supported by the NOAA MAPP drought project (NA17OAR4310144).

References

An, S. I., & Wang, B. (2000). Interdecadal change of the structure of the ENSO mode and its impact on the ENSO frequency. *Journal of Climate*, *13*, 2044–2055. https://doi.org/10.1175/1520-0442

Barnston, A. G., Chelliah, M., & Goldenberg, S. B. (1997). Documentation of a highly ENSO-related SST region in the equatorial Pacific. *Atmosphere-Ocean*, *35*, 367–383.

Barnston, A. G., Tippett, M. K., L'Heureux, M. L., Li, S., & DeWitt, D. G. (2012). Skill of real-time seasonal ENSO model predictions during 2002—2011—Is our capability increasing? *Bulletin of the American Meteorological Society*, *93*(5), 631–651. https://doi.org/10.1175/BAMS-D-11-00111.1

Battisti, D. S. (1989). On the role of subtropical Rossby waves during ENSO. *Journal of Physical Oceanography*, *19*(4), 551–560. https://doi.org/10.1175/1520-0485(1989)0190551:OTROOE>2.0.CO;2

Behringer, D. W. (2007). The Global Ocean Data Assimilation System (GODAS) at NCEP. Preprints, 11th symposium on integrated observing and assimilation systems for atmosphere, oceans, and land surface, San Antonio, TX, Amer. Meteor. Soc., 3.3. Retrieved from http://ams.confex.com/ams/87ANNUAL/techprogram/paper_119541.htm, 16 January, 2007.

Bunge, L., & Clarke, A. J. (2014). On the warm water volume and its changing relationship with ENSO. *Journal of Physical Oceanography*, *44*(5), 1372–1385. https://doi.org/10.1175/JPO-D-13-062.1

Chen, H.-C., Hu, Z.-Z., Huang, B., & Sui, C.-H. (2016). The role of reversed equatorial zonal transport in terminating an ENSO event. *Journal of Climate*, *29*(16), 5859–5877. https://doi.org/10.1175/JCLI-D-16-0047.1

Chen, H.-C., & Jin, F.-F. (2020). Fundamental behavior of ENSO phase locking. *Journal of Climate*, *33*(5), 1953–1968. https://doi.org/10.1175/JCLI-D-19-0264.1

Chen, H.-C., Tseng, Y.-H., Hu, Z.-Z., & Ding, R. (2020). Enhancing the ENSO predictability beyond the spring barrier. *Scientific Reports*, *10*(1), 984. https://doi.org/10.1038/s41598-020-57853-7

Clarke, A. J. (2010). Analytical theory for the quasi-steady and low-frequency equatorial ocean response to wind forcing: The 'tilt' and 'warm water volume' modes. *Journal of Physical Oceanography*, *40*(1), 121–137. https://doi.org/10.1175/2009JPO4263.1

Clarke, A. J., & van Gorder, S. (2001). ENSO prediction using an ENSO trigger and a proxy for western equatorial Pacific warm pool movement. *Geophysical Research Letters*, *28*(4), 579–582. https://doi.org/10.1029/2000GL012201

England, M. H., McGregor, S., Spence, P., Meehl, G. A., Timmermann, A., Cai, W., et al. (2014). Recent intensification of wind-driven circulation in the Pacific and the ongoing warming hiatus. *Nature Climate Change*, *4*, 222–227. https://doi.org/10.1038/nclimate2106

Goddard, L., & Philander, S. G. H. (2001). The energetics of El Niño and La Niña. *Journal of Climate*, *13*, 1496–1516.

Horii, T., Ueki, I., & Hanawa, K. (2012). Breakdown of ENSO predictors in the 2000s: Decadal changes of recharge/discharge–SST phase relation and atmospheric intraseasonal forcing. *Geophysical Research Letters*, *39*, L10707. https://doi.org/10.1029/2012GL051740

Hu, Z.-Z., Huang, B., Zhu, J., Kumar, A., & McPhaden, M. J. (2019). On the variety of coastal El Niño events. *Climate Dynamics*, *52*(12), 7537–7552. https://doi.org/10.1007/s00382-018-4290-4

Hu, Z.-Z., Kumar, A., & Huang, B. (2016). Spatial distribution and the interdecadal change of leading modes of heat budget of the mixed −layer in the tropical Pacific and the association with ENSO. *Climate Dynamics*, *46*(5−6), 1753–1768. https://doi.org/10.1007/s00382-015-2672-4

Hu, Z.-Z., Kumar, A., Huang, B., Zhu, J., L'Heureux, M., McPhaden, M. J., & Yu, J.-Y. (2020). The interdecadal shift of ENSO properties in 1999/2000: A review. *Journal of Climate*, *33*(11), 4441–4462. https://doi.org/10.1175/JCLI-D-19-0316.1

Hu, Z.-Z., Kumar, A., Huang, B., Zhu, J., Zhang, R.-H., & Jin, F.-F. (2017). Asymmetric evolution of El Niño and La Niña: The recharge/discharge processes and role of the off-equatorial sea surface height anomaly. *Climate Dynamics*, *49*(7–8), 2737–2748. https://doi.org/10.1007/s00382-016-3498-4

Hu, Z.-Z., Kumar, A., Jha, B., & Huang, B. (2020). How much of monthly mean precipitation variability over global land is associated with SST anomalies? *Climate Dynamics*, *54*(1–2), 701–712. https://doi.org/10.1007/s00382-019-05023-5

Hu, Z.-Z., Kumar, A., Ren, H.-L., Wang, H., L'Heureux, M., & Jin, F.-F. (2013). Weakened interannual variability in the tropical Pacific Ocean since 2000. *Journal of Climate*, *26*(8), 2601–2613. https://doi.org/10.1175/JCLI-D-12-00265.1

Hu, Z.-Z., Kumar, A., Xue, Y., & Jha, B. (2014). Why were some La Niñas followed by another La Niña? *Climate Dynamics*, *42*(3–4), 1029–1042. https://doi.org/10.1007/s00382-013-1917-3

Hu, Z.-Z., Kumar, A., Zhu, J., Huang, B., Tseng, Y.-H., & Wang, X. (2017). On the shortening of the lead time of ocean warm water volume to ENSO SST since 2000. *Scientific Reports*, *7*(1), 4294. https://doi.org/10.1038/s41598-017-04566-z

Hu, Z.-Z., McPhaden, M. J., Kumar, A., Yu, J.-Y., & Johnson, N. C. (2020). Uncoupled El Niño warming. *Geophysical Research Letters*, *47*. https://doi.org/10.1029/2020GL087621

Hu, Z.-Z., & Nitta, T. (1996). Wavelet analysis of summer rainfall over North China and India and SOI using 1891–1992 data. *Journal of the Meteorological Society of Japan*, *74*(6), 833–844. https://doi.org/10.2151/jmsj1965.74.6_833

Izumo, T., Lengaigne, M., Vialard, J., Suresh, I., & Planton, Y. (2019). On the physical interpretation of the lead relation between Warm Water Volume and the El Niño Southern Oscillation. *Climate Dynamics*, *52*(5-6), 2923–2942. https://doi.org/10.1007/s00382-018-4313-1

Jin, F.-F. (1997a). An equatorial ocean recharge paradigm for ENSO. Part I: Conceptual model. *Journal of the Atmospheric Sciences*, *54*(7), 811–829. https://doi.org/10.1175/1520-0469(1997)0540811:AEORPF>2.0.CO;2

Jin, F.-F. (1997b). An equatorial ocean recharge paradigm for ENSO. Part II: A stripped-down coupled model. *Journal of the Atmospheric Sciences*, *54*(7), 830–847. https://doi.org/10.1175/1520-0469(1997)0540830:AEORPF>2.0.CO;2

Kanamitsu, M., Ebisuzaki, W., Woollen, J., Yang, S. K., Hnilo, J. J., Fiorino, M., & Potter, G. L. (2002). NCEP−DOE AMIP−II reanalysis (R−2). *Bulletin of the American Meteorological Society*, *83*(11), 1631–1644. https://doi.org/10.1175/BAMS-83-11-1631

Kao, H.-Y., & Yu, J.-Y. (2009). Contrasting eastern-Pacific and central-Pacific types of ENSO. *Journal of Climate*, *22*(3), 615–632. https://doi.org/10.1175/2008JCLI2309.1

Kessler, W. S. (2002). Is ENSO a cycle or a series of events? *Geophysical Research Letters*, *29*(23), 2125. https://doi.org/10.1029/2002GL015924

Köberle, C., & Philander, S. G. H. (1994). On the processes that control seasonal variations of sea surface temperatures in the tropical Pacific Ocean. *Tellus A*, *46*(4), 481–496. https://doi.org/10.3402/tellusa.v46i4.15494

Kug, J.-S., An, S. I., Jin, F. F., & Kang, I. S. (2005). Preconditions for El Niño and La Niña onsets and their relation to the Indian Ocean. *Geophysical Research Letters*, *32*, L05706. https://doi.org/10.1029/2004GL021674

Kug, J.-S., Jin, F.-F., & An, S.-I. (2009). Two types of El Niño events: Cold tongue El Niño and warm pool El Niño. *Journal of Climate*, *22*(6), 1499–1515. https://doi.org/10.1175/2008JCLI2624.1

Kumar, A., & Hu, Z.-Z. (2014). Interannual and interdecadal variability of ocean temperature along the equatorial Pacific in conjunction with ENSO. *Climate Dynamics*, *42*(5–6), 1243–1258. https://doi.org/10.1007/s00382-013-1721-0

Li, X., Hu, Z.-Z., & Becker, E. (2019). On the westward shift of tropical Pacific climate variability since 2000. *Climate Dynamics*, *53*(5–6), 2905–2918. https://doi.org/10.1007/s00382-019-04666-8

Lübbecke, J. F., & McPhaden, M. J. (2014). Assessing the 21st century shift in ENSO variability in terms of the Bjerknes stability index. *Journal of Climate*, *27*(7), 2577–2587. https://doi.org/10.1175/JCLI-D-13-00438.1

McPhaden, M. J. (2003). Tropical Pacific Ocean heat content variations and ENSO persistence barriers. *Geophysical Research Letters*, *30*(9), 1480. https://doi.org/10.1029/2003GL016872

McPhaden, M. J. (2012). A 21st century shift in the relationship between ENSO SST and warm water volume anomalies. *Geophysical Research Letters*, *39*, L09706. https://doi.org/10.1029/2012GL051826

McPhaden, M. J., Lee, T., & McClurg, D. (2011). El Niño and its relationship to changing background conditions in the tropical Pacific Ocean. *Geophysical Research Letters*, *38*, L15709. https://doi.org/10.1029/2011GL048275

McPhaden, M. J., Zhang, X., Hendon, H. H., & Wheeler, M. C. (2006). Large scale dynamics and MJO forcing of ENSO variability. *Geophysical Research Letters*, *33*, L16702. https://doi.org/10.1029/2006GL026786

Meinen, C. S., & McPhaden, M. J. (2000). Observations of warm water volume changes in the equatorial Pacific and their relationship to El Niño and La Niña. *Journal of Climate*, *13*(20), 3551–3559. https://doi.org/10.1175/1520-0442

Meyers, S. D., Kelly, B. G., & O'Brien, J. J. (1993). An introduction to wavelet analysis in oceanography and meteorology: With application to the dispersion of Yanai waves. *Monthly Weather Review*, *121*(10), 2858–2866. https://doi.org/10.1175/1520-0493

Mitchell, T. P., & Wallace, J. M. (1992). On the annual cycle in equatorial convection and sea-surface temperature. *Journal of Climate*, *5*(10), 1140–1156. https://doi.org/10.1175/1520-0442(1992)0051140:TACIEC>2.0.CO;2

National Research Council (2010). Assessment of Intraseasonal to Interannual Climate Prediction and Predictability, 192 PP., ISBN-10: 0–309-15183-X, the National Academies Press, Washington, DC, USA.

Neske, S., & McGregor, S. (2018). Understanding the warm water volume precursor of ENSO events and its interdecadal variation. *Geophysical Research Letters*, *45*, 1577–1585. https://doi.org/10.1002/2017GL076439

Ren, H.-L., & Jin, F.-F. (2013). Recharge oscillator mechanisms in two types of ENSO. *Journal of Climate*, *26*(17), 6506–6523. https://doi.org/10.1175/JCLI-D-12-00601.1

Singh, A., & Delcroix, T. (2013). Eastern and central Pacific ENSO and their relationships to the recharge/discharge oscillator paradigm. *Deep-Sea Research Part I*, *82*, 32–43. https://doi.org/10.1016/j.dsr.2013.08.002

Torrence, C., & Webster, P. J. (1998). The annual cycle of persistence in the El Niño-Southern Oscillation. *Quarterly Journal of the Royal Meteorological Society*, *124*(550), 1985–2004. https://doi.org/10.1002/qj.49712455010

Tseng, Y.-H., Hu, Z. Z., Ding, R., & Chen, H. C. (2016). An ENSO prediction approach based on ocean conditions and ocean–atmosphere coupling. *Climate Dynamics*, *48*(5–6), 2025–2044. https://doi.org/10.1007/s00382-016-3188-2

Wang, B. (1995). Interdecadal changes in El Niño onset in the last four decades. *Journal of Climate*, *8*(2), 267–285. https://doi.org/10.1175/1520-0442(1995)0080267:ICIENO>2.0.CO;2

Wang, C., Deser, C., Yu, J.-Y., Di Nezio, P., & Clement, A. (2016). El Niño-Southern Oscillation (ENSO): A review. In P. Glymn, D. Manzello, & I. Enochs (Eds.), *Coral Reefs of the Eastern Pacific* (pp. 85–106). New York: Springer Science Publisher.

Wang, W., Chen, M., & Kumar, A. (2010). An assessment of the CFS real-time seasonal forecasts. *Weather and Forecasting*, *25*(3), 950–969. https://doi.org/10.1175/2010WAF2222345.1

Webster, P. J., & Yang, S. (1992). Monsoon and ENSO: Selectively interactive system. *Quarterly Journal of the Royal Meteorological Society*, *118*, 877–926. https://doi.org/10.1002/qj.49711850705

Wen, C., Kumar, A., Xue, Y., & McPhaden, M. J. (2014). Changes in tropical Pacific thermocline depth and their relationship to ENSO after 1999. *Journal of Climate*, *27*(19), 7230–7249. https://doi.org/10.1175/JCLI-D-13-00518.1

Wyrtki, K. (1985). Water displacements in the Pacific and the genesis of El Niño cycles. *Journal of Geophysical Research*, *90*(C4), 7129–7132. https://doi.org/10.1029/JC090iC04p07129

Xiang, B., Wang, B., & Li, T. (2013). A new paradigm for the predominance of standing Central Pacific warming after the late 1990s. *Climate Dynamics*, *41*(2), 327–340. https://doi.org/10.1007/s00382-012-1427-8

Xie, S.-P. (1994). Oceanic response to the wind forcing associated with the Intertropical convergence zone in the northern hemisphere. *Journal of Geophysical Research*, *99*(C10), 20393. https://doi.org/10.1029/94JC01653

Zhang, W., Li, S., Jin, F.-F., Xie, R., Liu, C., Stuecker, M. F., & Xue, A. (2019). ENSO regime changes responsible for decadal phase relationship variations between ENSO sea surface temperature and warm water volume. *Geophysical Research Letters*, *46*, 7546–7553. https://doi.org/10.1029/2019GL082943